

# Specific Loss Power in Magnetic Hyperthermia: Comparison of Monodispersion and Polydispersion

Kenya Murase<sup>#1</sup>

<sup>#</sup>Department of Medical Physics and Engineering, Division of Medical Technology and Science, Faculty of Health Science, Graduate School of Medicine, Osaka University, Suita, Osaka, Japan

## Abstract

Magnetic hyperthermia (MH) is a promising approach to cancer therapy that uses the heat released by magnetic nanoparticles (MNPs) under an alternating magnetic field (AMF). Since the existence of some size polydispersity of MNPs is experimentally unavoidable, the size polydispersity is important for achieving an accurate control of the heating performance of MNPs. The purpose of this study was to investigate the effect of the size polydispersity on the specific loss power (SLP) in MH under various conditions of MNPs, AMF, and static magnetic field (SMF). The SLP value in the quasi steady state ( $SLP_{qss}$ ) for the polydisperse case was computed using the probability density function based on a log-normal distribution. The  $SLP_{qss}$  value was largely affected by the size polydispersity and its dependency on the size polydispersity changed depending on the magnetic and physical properties of MNPs and the parameters of AMF. The plot of the  $SLP_{qss}$  values against the position from a field-free point was also affected by the size polydispersity. Our results suggest that it is essential to consider the size polydispersity for the accurate estimation of SLP and for accurately controlling the temperature rise and the area of local heating in MH using SMF.

**Keywords** —Magnetic hyperthermia, magnetic nanoparticle, specific loss power, monodispersion, polydispersion, log-normal distribution.

## I. INTRODUCTION

Magnetic hyperthermia is a promising approach to cancer therapy that uses the heat released by magnetic nanoparticles (MNPs) under an alternating magnetic field (AMF) to treat tumors [1]-[3]. With the development of precise methods for synthesizing functionalized MNPs [4], MNPs with functionalized surfaces, which have high specificity for tumors, have been developed as heating elements for magnetic hyperthermia [5]. Recently, MNPs with a higher heating efficiency, *i.e.*, specific loss power (SLP) have also been actively developed [6].

The estimation of SLP is important for evaluating the heating efficiency of MNPs, for optimizing the parameters of AMF, and for the optimal design of MNPs in an attempt to establish the effectiveness of magnetic hyperthermia [7], [8]. It is

also important to heat the targeted tumor to the desired temperature without damaging the surrounding healthy tissues in order to enhance the effectiveness of magnetic hyperthermia [7], [8]. Tasci *et al.* [9] proposed and designed a system that focuses the heat into very small regions using a static magnetic field (SMF) with a field-free point (FFP) generated by two solenoid coils, and reported that this method will be useful for making magnetic hyperthermia a more effective approach to cancer therapy with a decreased risk of heating surrounding healthy tissues. We have also investigated the usefulness of this method and reported that it is useful for controlling the temperature rise in magnetic hyperthermia [10].

Recently, we have presented methods for estimating SLP and compared the SLP values estimated by these methods under various conditions of MNPs and AMF [8]. Furthermore, we have also presented a method for estimating the SLP in the presence of both the AMF and SMF [11], which was based on the numerical solution of the magnetization relaxation equation of Shliomis [12]. In our previous papers [8], [11], however, the particle size distribution was assumed to be monodisperse. As pointed out by Munoz-Menendez *et al.* [13], [14], the existence of some size polydispersity of MNPs is experimentally unavoidable, resulting in a different hyperthermia performance depending on the size of each MNP. Thus, the size polydispersity of MNPs is one of the important issues to achieve an accurate control of the heating performance of MNPs.

Our purpose in this study was to investigate the effect of the size polydispersity on the SLP in magnetic hyperthermia in comparison with the monodisperse case under various conditions of MNPs, AMF, and SMF.

## II. MATERIALS AND METHODS

### A. Theory

The magnetization relaxation equation of Shliomis [12], [15] is given by

$$\frac{d\mathbf{M}}{dt} = \mathbf{\Omega} \times \mathbf{M} - \frac{\mathbf{M} - \mathbf{M}_0}{\tau} - \frac{\mathbf{M} \times (\mathbf{M} \times \mathbf{H})}{6\eta\phi}, \quad (1)$$

Where  $\mathbf{M}$  is the magnetization of MNPs under the magnetic field  $\mathbf{H}$ ,  $\mathbf{\Omega}$  is the flow velocity,  $\phi$  is the volume fraction, and  $\eta$  is the viscosity of the suspending fluid. When there is no bulk flow and  $\mathbf{M}$

and  $\mathbf{H}$  are collinear, Eq. (1) is reduced to the following equation [7]:

$$\frac{dM(t)}{dt} = -\frac{M(t)-M_0(t)}{\tau} \quad (2)$$

In Eq. (2),  $\tau$  is the effective relaxation time given by

$$\frac{1}{\tau} = \frac{1}{\tau_N} + \frac{1}{\tau_B} \quad (3)$$

where  $\tau_N$  and  $\tau_B$  are the Néel relaxation and Brownian relaxation time, respectively [6].  $\tau_N$  and  $\tau_B$  are given by the following relationships [7]:

$$\tau_N = \tau_0 \frac{\sqrt{\pi} e^{\Gamma}}{2\sqrt{\Gamma}} \quad (4)$$

and

$$\tau_B = \frac{3\eta V_H}{k_B T} \quad (5)$$

respectively, where  $\tau_0$  is the average relaxation time in response to a thermal fluctuation,  $k_B$  is the Boltzmann constant,  $T$  is the temperature, and  $\Gamma = KV_M/(k_B T)$ , with  $K$  being the anisotropy constant of MNP.  $V_H$  is taken as the hydrodynamic volume of MNP that is larger than the magnetic volume  $V_M = \pi D^3/6$  for MNP of diameter  $D$ . As a model for  $V_H$ , it is assumed that  $V_H = (1 + 2\delta/D)^3 V_M$ , where  $\delta$  is the thickness of a sorbed surfactant layer [6].  $M_0(t)$  in Eq. (2) denotes the equilibrium magnetization and is given by

$$M_0(t) = \chi_0 H(t) \quad (6)$$

where  $\chi_0$  and  $H(t)$  are the equilibrium susceptibility and magnetic field strength at time  $t$ , respectively. In this study,  $H(t)$  was assumed to be

$$H(t) = H_0 \cos(2\pi f t) + H_s \quad (7)$$

where  $H_0$  and  $f$  denote the amplitude and frequency of AMF, respectively, and  $H_s$  denotes the strength of an external SMF. Because the actual equilibrium susceptibility ( $\chi_0$ ) is dependent on the magnetic field,  $\chi_0$  was assumed to be the chord susceptibility corresponding to the Langevin equation, given by [7]

$$\chi_0 = \chi_i \frac{3}{\xi} \left( \coth \xi - \frac{1}{\xi} \right) \quad (8)$$

where  $\chi_i$  is the initial susceptibility given by  $\chi_i = \mu_0 \phi M_d^2 V_M / (3k_B T)$ ,  $\xi$  is the Langevin parameter given by  $\xi = \mu_0 M_d H V_M / (k_B T)$ ,  $M_d$  is the domain magnetization of a suspended particle, and  $\mu_0$  is the permeability of free space. It should be noted that  $\xi$  is magnetic field dependent and thus time dependent.

Solving Eq. (2) and using Eq. (6) and Eq. (7) yield [8], [11]

$$M(t) = \frac{1}{\tau} e^{-\frac{t}{\tau}} \otimes M_0(t) + M(0) e^{-\frac{t}{\tau}} = \frac{1}{\tau} e^{-\frac{t}{\tau}} \otimes$$

$$\chi_0 [H_0 \cos(2\pi f t) + H_s] + M(0) e^{-\frac{t}{\tau}} \quad (9)$$

where  $\otimes$  denotes the convolution integral and  $M(0)$  is  $M(t)$  at  $t = 0$ . In this study,  $M(0)$  was assumed to be  $M(0) = M_0(0) = \chi_0(H_0 + H_s)$ . When  $t = \infty$ , however, the second term of the right-hand side of Eq. (9) can be neglected.

The average rate of energy dissipation per cycle of the period, *i.e.*,  $1/f$  ( $\langle P \rangle$ ) is given by [7]

$$\langle P \rangle = -\mu_0 f \int_0^{1/f} M(t) \frac{dH(t)}{dt} dt \quad (10)$$

Substituting Eq. (7) into Eq. (10) yields

$$\langle P \rangle = 2\pi\mu_0 H_0 f^2 \int_0^{1/f} M(t) \sin(2\pi f t) dt \quad (11)$$

The rate of energy dissipation per unit mass of MNPs, *i.e.*, SLP can be obtained from  $\langle P \rangle$  as [8], [11]

$$SLP = \frac{\langle P \rangle}{\phi \rho} \quad (12)$$

where  $\rho$  is the density of suspending fluid.

Because  $M(t)$  given by Eq. (9) must be time-periodic in the steady state, the SLP value for the  $i$ -th cycle ( $SLP_i$ ) can be given by [8], [11]

$$SLP_i = \frac{2\pi\mu_0 H_0 f^2}{\phi \rho} \left\{ \int_{(i-1)/f}^{i/f} \left[ \frac{1}{\tau} e^{-\frac{t}{\tau}} \otimes M_0(t) \right] \sin(2\pi f t) dt + 2\pi f \tau M_0 + 2\pi f \tau 2e^{-if\tau} (e1f\tau - 1) \right\} \quad (13)$$

It should be noted that when  $i$  is sufficiently large, the second term of the right-hand side of Eq. (13) can be neglected and  $SLP_i$  approaches the steady state. We denote the  $SLP_i$  value in the quasi steady state by  $SLP_{qss}$ . Actually,  $SLP_{qss}$  was taken as the  $SLP_i$  value in the case when the relative error given by  $|SLP_i - SLP_{i-1}|/SLP_{i-1}$  was less than  $10^{-10}$  [11]. The integration in Eq. (13) was performed by use of the trapezoidal rule [17] (“trapz” in MATLAB®; The MathWorks, Inc., Natick, MA, USA) and the convolution integral was calculated using the MATLAB® function (“conv”).

Because not all particles in a certain volume have the same diameter  $D$  in the polydisperse case [13], [14], the  $SLP_{qss}$  value calculated from Eq. (13) should be averaged based on the particle size distribution as

$$\langle SLP_{qss} \rangle = \int_0^\infty SLP_{qss} \cdot PDF(D) dD \quad (14)$$

where  $PDF(D)$  denotes the probability density function of the particle size distribution. The result of a natural growth process during particle synthesis does not yield particles with a single diameter  $D$ , but with a polydisperse particle size distribution. A reasonable and commonly used approach for modeling is the log-normal distribution [17]. In this case,  $PDF(D)$  is given by

$$PDF(D) = \frac{1}{\sqrt{2\pi}\sigma D} \cdot \exp \left[ -\frac{1}{2} \left( \frac{\ln(D) - \mu}{\sigma} \right)^2 \right] \quad (15)$$

where  $\mu$  and  $\sigma$  denote the mean and standard deviation of the natural logarithm of  $D$ , respectively, and are given by

$$\mu = \ln(mD) - \frac{1}{2} \ln \left( \frac{sD^2}{mD^2} + 1 \right) \quad (16)$$

and

$$\sigma = \sqrt{\ln \left( \frac{sD^2}{mD^2} + 1 \right)} \quad (17)$$

respectively.  $mD$  and  $sD$  denote the mean and standard deviation of  $D$ , respectively. When  $mD$  and  $\sigma$  are known,  $sD$  is given by

$$sD = mD \cdot \sqrt{e^{\sigma^2} - 1} \quad (18)$$

The derivative of  $\langle SLP_{qss} \rangle$  with respect to  $D$  is given by

$$\frac{d\langle SLP_{qss} \rangle}{dD} = SLP_{qss} \cdot PDF(D) \quad (19)$$

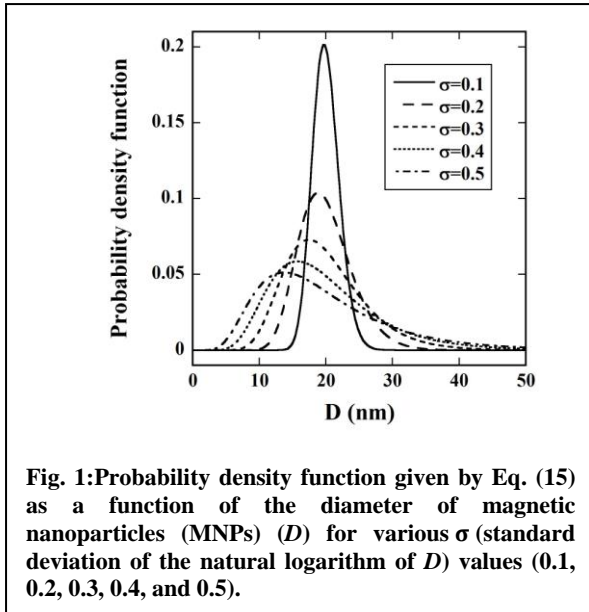


**Fig. 1:**Probability density function given by Eq. (15) as a function of the diameter of magnetic nanoparticles (MNP) ( $D$ ) for various  $\sigma$  (standard deviation of the natural logarithm of  $D$ ) values (0.1, 0.2, 0.3, 0.4, and 0.5).

It should be noted that when  $\sigma$  approaches zero,  $PDF(D)$  given by Eq. (15) approaches  $\delta(D - mD)$ , where  $\delta(*)$  denotes the so-called Dirac's delta function. When  $\sigma = 0$ ,  $\langle SLP_{qss} \rangle$  given by Eq. (14) corresponds to the  $SLP_{qss}$  value for the monodisperse case, which is denoted by  $SLP_{qss}^{mono}$  in this study.

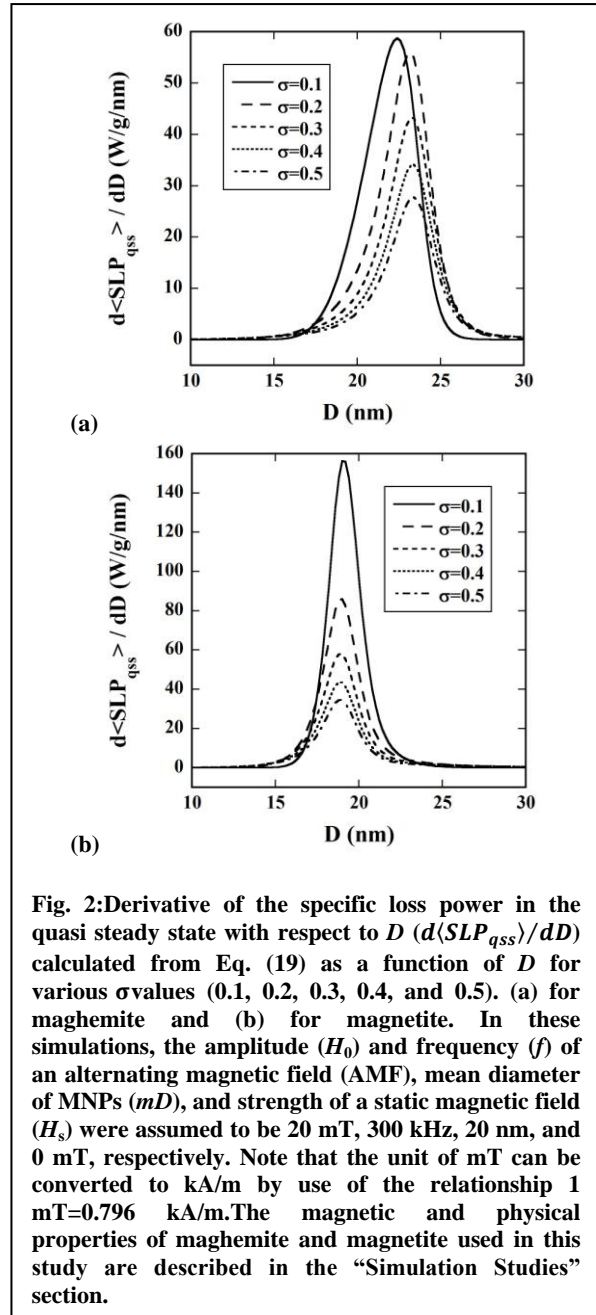
**B. Simulation Studies**

In this study, we assumed that MNPs consisted of two kinds of iron oxide nanoparticles, *i.e.*, maghemite ( $\gamma\text{-Fe}_2\text{O}_3$ ) and magnetite ( $\text{Fe}_3\text{O}_4$ ). We fixed  $\tau_0, \delta, M_d, K, \eta, \rho, \phi$ , and  $T$  to be  $10^{-9}$  s, 2 nm, 414 kA/m,  $4.7 \text{ kJ/m}^3$ ,  $0.00235 \text{ kg/m}^3$ ,  $4600 \text{ kg/m}^3$ , 0.003, and  $37^\circ\text{C}$ , respectively, for maghemite [17], [18]. For magnetite, we fixed  $\tau_0, \delta, M_d, K, \eta, \rho, \phi$ , and  $T$  to be  $10^{-9}$  s, 2 nm, 446 kA/m,  $9.0 \text{ kJ/m}^3$ ,  $0.00235 \text{ kg/m}^3$ ,  $5180 \text{ kg/m}^3$ , 0.003, and  $37^\circ\text{C}$ , respectively [18]. When  $H_0, f$ , and  $mD$  were fixed, they were taken as 20 mT, 300 kHz, and 20 nm, respectively. It should be noted that the unit of mT can be converted to kA/m by use of the relationship  $1 \text{ mT} = 0.796 \text{ kA/m}$ .

When considering the control of the temperature rise using the SMF with a gradient strength of  $G_s$ , the strength of the SMF at a distance of  $x$  from the FFP ( $H_s(x)$ ) was given by  $H_s(x) = G_s \times x$  [11].

**III. RESULTS**

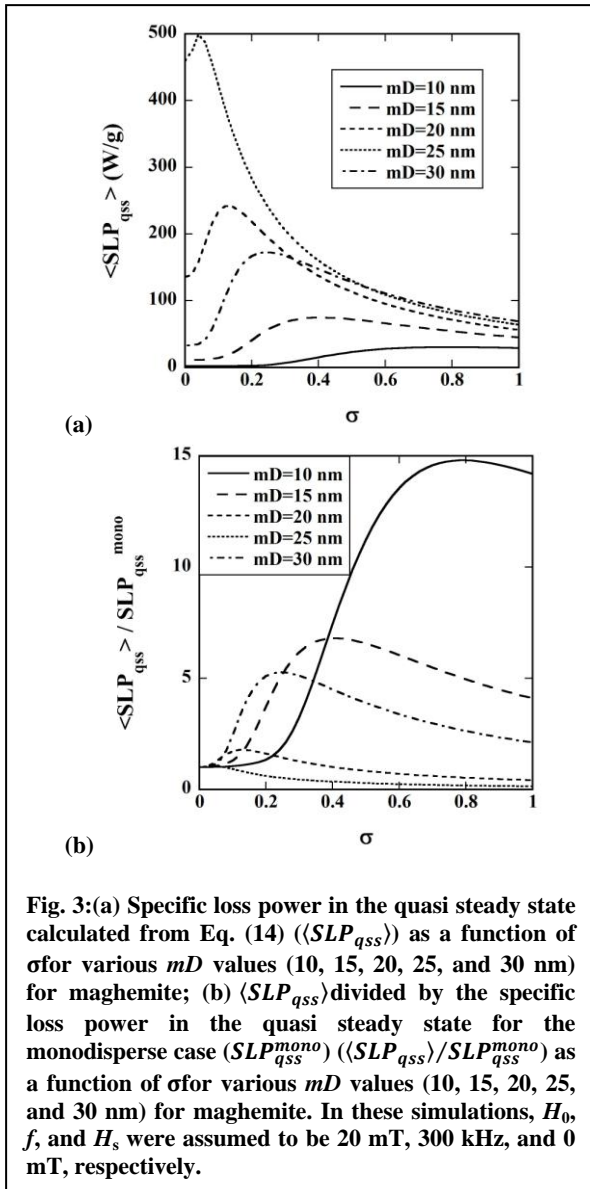
Fig. 1 shows  $PDF(D)$  given by Eq. (15) as a function of  $D$  for various  $\sigma$  values (0.1, 0.2, 0.3, 0.4, and 0.5). Fig. 2 shows the derivative of the specific loss power in the quasi steady state with respect to  $D$  ( $d\langle SLP_{qss} \rangle / dD$ ) calculated from Eq. (19) as a function of  $D$  for various  $\sigma$  values (0.1, 0.2, 0.3, 0.4, and 0.5). Fig. 2(a) and Fig. 2(b) show cases for maghemite and magnetite, respectively. In these simulations,  $H_0, f, mD$ , and  $H_s$  were assumed to be 20 mT, 300 kHz, 20 nm, and 0 mT, respectively. As shown in Fig. 2, the plots for maghemite had peaks between  $D = 22 \text{ nm}$  and  $D = 25 \text{ nm}$  (Fig. 2(a)), whereas those for magnetite had peaks near  $D =$



**Fig. 2:**Derivative of the specific loss power in the quasi steady state with respect to  $D$  ( $d\langle SLP_{qss} \rangle / dD$ ) calculated from Eq. (19) as a function of  $D$  for various  $\sigma$  values (0.1, 0.2, 0.3, 0.4, and 0.5). (a) for maghemite and (b) for magnetite. In these simulations, the amplitude ( $H_0$ ) and frequency ( $f$ ) of an alternating magnetic field (AMF), mean diameter of MNPs ( $mD$ ), and strength of a static magnetic field ( $H_s$ ) were assumed to be 20 mT, 300 kHz, 20 nm, and 0 mT, respectively. Note that the unit of mT can be converted to kA/m by use of the relationship  $1 \text{ mT} = 0.796 \text{ kA/m}$ . The magnetic and physical properties of maghemite and magnetite used in this study are described in the “Simulation Studies” section.

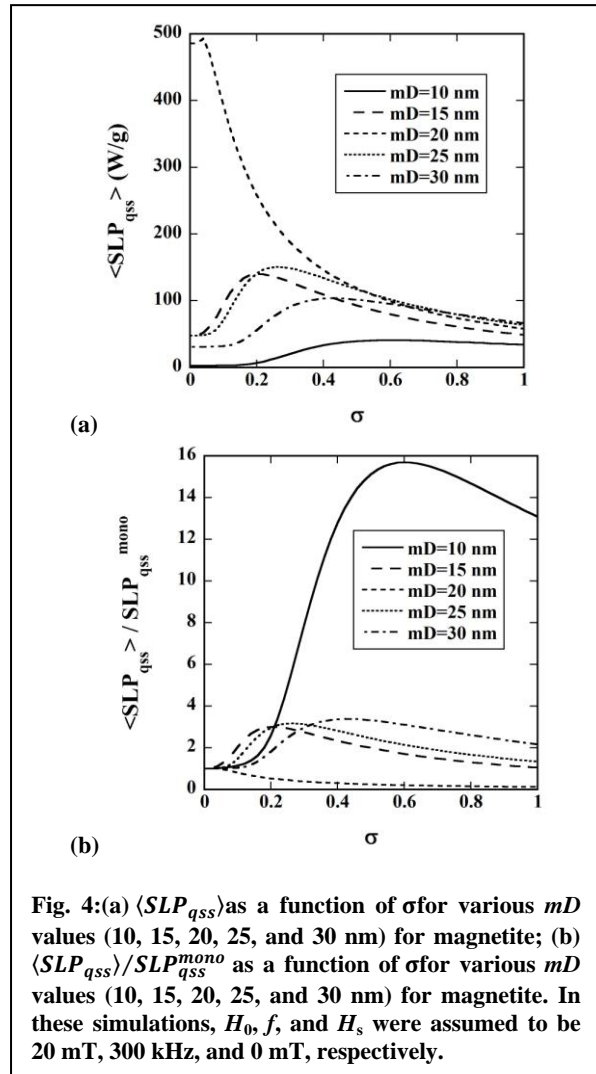
20 nm (Fig. 2(b)). Although the height, width, and position of the peaks differed between maghemite (Fig. 2(a)) and magnetite (Fig. 2(b)), the height of the peaks decreased with increasing  $\sigma$  value in both cases.

Fig. 3(a) shows the  $\langle SLP_{qss} \rangle$  value calculated from Eq. (14) as a function of  $\sigma$  for various  $mD$  values (10, 15, 20, 25, and 30 nm) for maghemite, whereas Fig. 3(b) shows the  $\langle SLP_{qss} \rangle$  value divided by the  $SLP_{qss}$  value for the monodisperse case ( $SLP_{qss}^{mono}$ ) ( $\langle SLP_{qss} \rangle / SLP_{qss}^{mono}$ ) as a function of  $\sigma$  for various  $mD$  values (10, 15, 20, 25, and 30 nm). Fig. 4 shows those for magnetite. In these simulations,  $H_0, f$ , and  $H_s$  were assumed to be 20 mT, 300 kHz, and 0 mT, respectively. As shown in Fig. 3 and Fig. 4, the dependencies of  $\langle SLP_{qss} \rangle$  and  $\langle SLP_{qss} \rangle / SLP_{qss}^{mono}$  on  $\sigma$  changed largely depending on  $mD$ . In the case of maghemite (Fig. 3), when  $mD$  was 25 nm, both



**Fig. 3:**(a) Specific loss power in the quasi steady state calculated from Eq. (14) ( $\langle SLP_{qss} \rangle$ ) as a function of  $\sigma$  for various  $mD$  values (10, 15, 20, 25, and 30 nm) for maghemite; (b)  $\langle SLP_{qss} \rangle$  divided by the specific loss power in the quasi steady state for the monodisperse case ( $SLP_{qss}^{mono}$ ) ( $\langle SLP_{qss} \rangle / SLP_{qss}^{mono}$ ) as a function of  $\sigma$  for various  $mD$  values (10, 15, 20, 25, and 30 nm) for maghemite. In these simulations,  $H_0$ ,  $f$ , and  $H_s$  were assumed to be 20 mT, 300 kHz, and 0 mT, respectively.

$\langle SLP_{qss} \rangle$  and  $\langle SLP_{qss} \rangle / SLP_{qss}^{mono}$  decreased almost monotonically with increasing  $\sigma$  value. When  $mD$  deviated from 25 nm, they increased with increasing  $\sigma$  value, making peaks, and then decreased thereafter. The  $\sigma$  values at which they had peaks changed depending on  $mD$ . In the case of magnetite (Fig. 4), when  $mD$  was 20 nm, both  $\langle SLP_{qss} \rangle$  and  $\langle SLP_{qss} \rangle / SLP_{qss}^{mono}$  decreased almost monotonically with increasing  $\sigma$  value. When  $mD$  deviated from 20 nm, they increased with increasing  $\sigma$  value, making peaks, and then decreased thereafter.



**Fig. 4:**(a)  $\langle SLP_{qss} \rangle$  as a function of  $\sigma$  for various  $mD$  values (10, 15, 20, 25, and 30 nm) for magnetite; (b)  $\langle SLP_{qss} \rangle / SLP_{qss}^{mono}$  as a function of  $\sigma$  for various  $mD$  values (10, 15, 20, 25, and 30 nm) for magnetite. In these simulations,  $H_0$ ,  $f$ , and  $H_s$  were assumed to be 20 mT, 300 kHz, and 0 mT, respectively.

monotonically with increasing  $\sigma$  value in the case of magnetite (Fig. 6). The  $\langle SLP_{qss} \rangle / SLP_{qss}^{mono}$  value did not largely depend on  $H_0$  in both cases (Fig. 5(b) and Fig. 6(b)).

Fig. 7(a) and Fig. 7(b) show the  $\langle SLP_{qss} \rangle$  and  $\langle SLP_{qss} \rangle / SLP_{qss}^{mono}$  values, respectively, as a function of  $\sigma$  for various  $f$  values (200, 400, 600, 800, and 1000 kHz) for maghemite. Fig. 8 shows those for magnetite. In these simulations,  $H_0$ ,  $mD$ , and  $H_s$  were assumed to be 20 mT, 20 nm, and 0 mT, respectively. As shown in Fig. 7 and Fig. 8, both  $\langle SLP_{qss} \rangle$  and  $\langle SLP_{qss} \rangle / SLP_{qss}^{mono}$  changed largely depending on  $f$  in both cases, and their dependencies on  $f$  differed between maghemite (Fig. 7) and magnetite (Fig. 8).

Fig. 9(a) and Fig. 9(b) show the  $\langle SLP_{qss} \rangle$  and  $\langle SLP_{qss} \rangle / SLP_{qss}^{mono}$  values, respectively, as a function of  $\sigma$  for various  $H_s$  values (0, 10, 20, 30, and 40 mT) for maghemite. Fig. 10 shows those for magnetite. In these simulations,  $H_0$ ,  $f$ , and  $mD$  were assumed to be 20 mT, 300 kHz, and 20 nm, respectively. In the case of maghemite (Fig. 9), both  $\langle SLP_{qss} \rangle$  and  $\langle SLP_{qss} \rangle / SLP_{qss}^{mono}$  had peaks between  $\sigma = 0.1$  and  $\sigma = 0.2$ , whereas they decreased almost

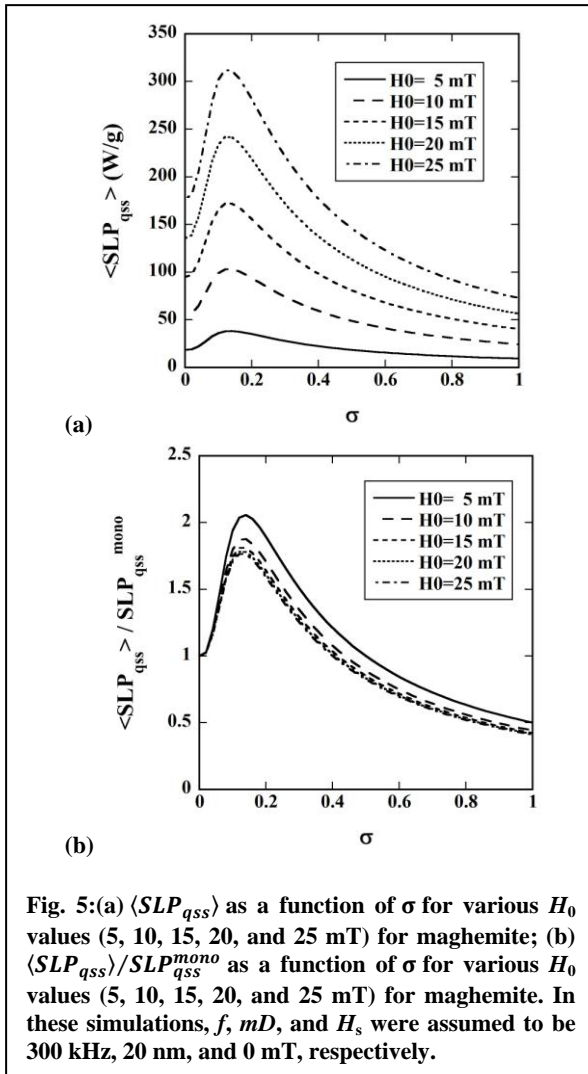


Fig. 5:(a)  $\langle SLP_{qss} \rangle$  as a function of  $\sigma$  for various  $H_0$  values (5, 10, 15, 20, and 25 mT) for maghemite; (b)  $\langle SLP_{qss} \rangle / SLP_{qss}^{mono}$  as a function of  $\sigma$  for various  $H_0$  values (5, 10, 15, 20, and 25 mT) for maghemite. In these simulations,  $f$ ,  $mD$ , and  $H_s$  were assumed to be 300 kHz, 20 nm, and 0 mT, respectively.

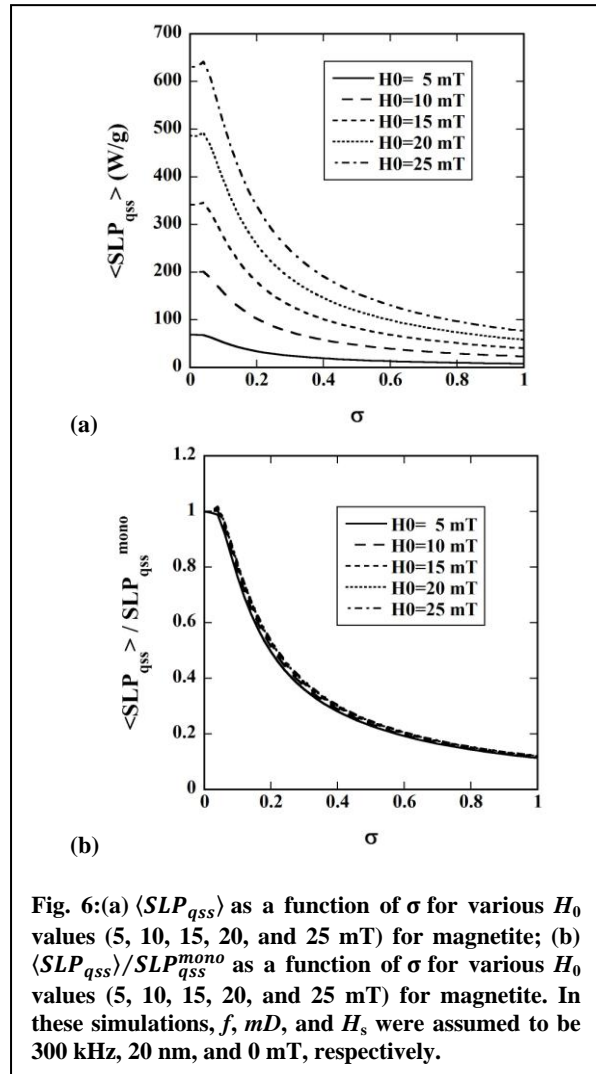


Fig. 6:(a)  $\langle SLP_{qss} \rangle$  as a function of  $\sigma$  for various  $H_0$  values (5, 10, 15, 20, and 25 mT) for magnetite; (b)  $\langle SLP_{qss} \rangle / SLP_{qss}^{mono}$  as a function of  $\sigma$  for various  $H_0$  values (5, 10, 15, 20, and 25 mT) for magnetite. In these simulations,  $f$ ,  $mD$ , and  $H_s$  were assumed to be 300 kHz, 20 nm, and 0 mT, respectively.

monotonically with increasing  $\sigma$  value in the case of magnetite (Fig. 10). The dependency of  $\langle SLP_{qss} \rangle / SLP_{qss}^{mono}$  on  $H_s$  differed between maghemite (Fig. 9(b)) and magnetite (Fig. 10(b)).

Fig. 11 shows the  $\langle SLP_{qss} \rangle$  values as a function of the distance from a field-free point ( $x$ ) for various  $\sigma$  values (0, 0.1, 0.2, 0.3, and 0.4). Fig. 11(a) and Fig.

11(b) show cases for maghemite and magnetite, respectively. In these simulations,  $H_0$ ,  $f$ ,  $mD$ , and  $G_s$  were assumed to be 20 mT, 300 kHz, 20 nm, and 2 T/m, respectively. As shown in Fig. 11, the plot of  $\langle SLP_{qss} \rangle$  against  $x$  changed largely depending on  $\sigma$  in both cases and its dependency on  $\sigma$  differed between maghemite (Fig. 11(a)) and magnetite (Fig. 11(b)).

#### IV. DISCUSSION

We previously investigated methods for estimating the SLP in magnetic hyperthermia under various conditions of MNPs and AMF [8]. We also presented a method for the estimation of the SLP in the presence of both the AMF and SMF [11], which was derived by solving the magnetization relaxation equation of Shliomis [12] numerically. In these studies, we assumed that the particle size distribution was monodisperse. As previously described, however, the existence of some size polydispersity of MNPs is experimentally unavoidable [13], [14]. Thus, in this study, we investigated the effect of the particle size polydispersity on the SLP in magnetic hyperthermia under various conditions of MNPs, AMF, and SMF. Our results (Fig. 3 to Fig. 11) demonstrated that the SLP

in magnetic hyperthermia largely depends on the particle size polydispersity, and suggest that it is essential to take into account the particle size polydispersity for the accurate estimation of SLP in magnetic hyperthermia.

In this study, we assumed that the particle size distribution obeys a log-normal distribution. As previously described, this assumption is commonly used and appears to be reasonable [17].

The derivative of  $\langle SLP_{qss} \rangle$  with respect to  $D$  given by Eq. (19), i.e.,  $d\langle SLP_{qss} \rangle / dD$  appears to represent the sensitivity of  $\langle SLP_{qss} \rangle$  to  $D$ . As shown in Fig. 2, although  $mD$  was assumed to be 20 nm, the peak of  $d\langle SLP_{qss} \rangle / dD$  was shifted to the larger  $D$  side in the case of maghemite (Fig. 2(a)), whereas that for magnetite had a peak near  $D=20$  nm (Fig. 2(b)). As

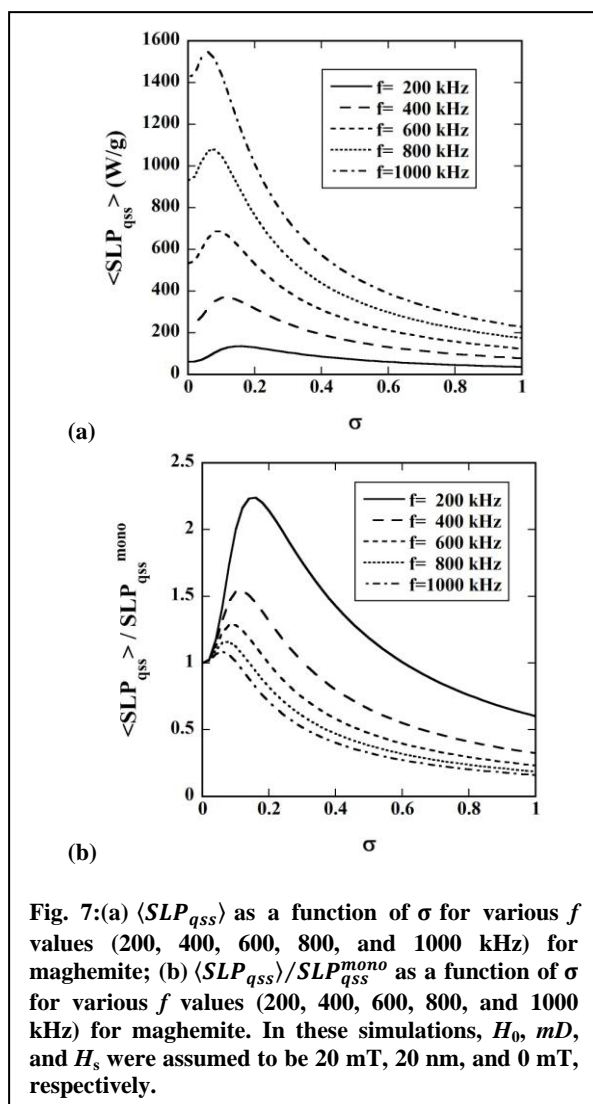


**Fig. 7:**(a)  $\langle SLP_{qss} \rangle$  as a function of  $\sigma$  for various  $f$  values (200, 400, 600, 800, and 1000 kHz) for maghemite; (b)  $\langle SLP_{qss} \rangle / SLP_{qss}^{mono}$  as a function of  $\sigma$  for various  $f$  values (200, 400, 600, 800, and 1000 kHz) for maghemite. In these simulations,  $H_0$ ,  $mD$ , and  $H_s$  were assumed to be 20 mT, 20 nm, and 0 mT, respectively.

previously described, the height of the peak decreased with increasing  $\sigma$  value in both cases. Furthermore, the plot of  $d\langle SLP_{qss} \rangle / dD$  against  $D$  for maghemite (Fig. 2(a)) was broader than that for magnetite (Fig. 2(b)). The height and width of these plots may be helpful in designing and/or synthesizing MNPs suitable for magnetic hyperthermia.

As shown in Fig. 3 and Fig. 4, the dependencies of  $\langle SLP_{qss} \rangle$  and  $\langle SLP_{qss} \rangle / SLP_{qss}^{mono}$  on  $\sigma$  changed largely depending on  $mD$ . In the case of maghemite (Fig. 3), when  $mD$  was 25 nm, both  $\langle SLP_{qss} \rangle$  and  $\langle SLP_{qss} \rangle / SLP_{qss}^{mono}$  decreased almost monotonically with increasing  $\sigma$  value. When  $mD$  deviated from 25 nm, they increased with increasing  $\sigma$  value, making peaks, and then decreased thereafter. In the case of magnetite (Fig. 4), when  $mD$  was 20 nm, both  $\langle SLP_{qss} \rangle$  and  $\langle SLP_{qss} \rangle / SLP_{qss}^{mono}$  decreased almost monotonically with increasing  $\sigma$  value, whereas they had peaks when  $mD$  deviated from 20 nm. The  $mD$  values of 25 nm for maghemite and 20 nm for magnetite approximately correspond to  $D$  at which  $d\langle SLP_{qss} \rangle / dD$  has a peak (Fig. 2). Thus, the above findings may suggest that  $d\langle SLP_{qss} \rangle / dD$  is a useful

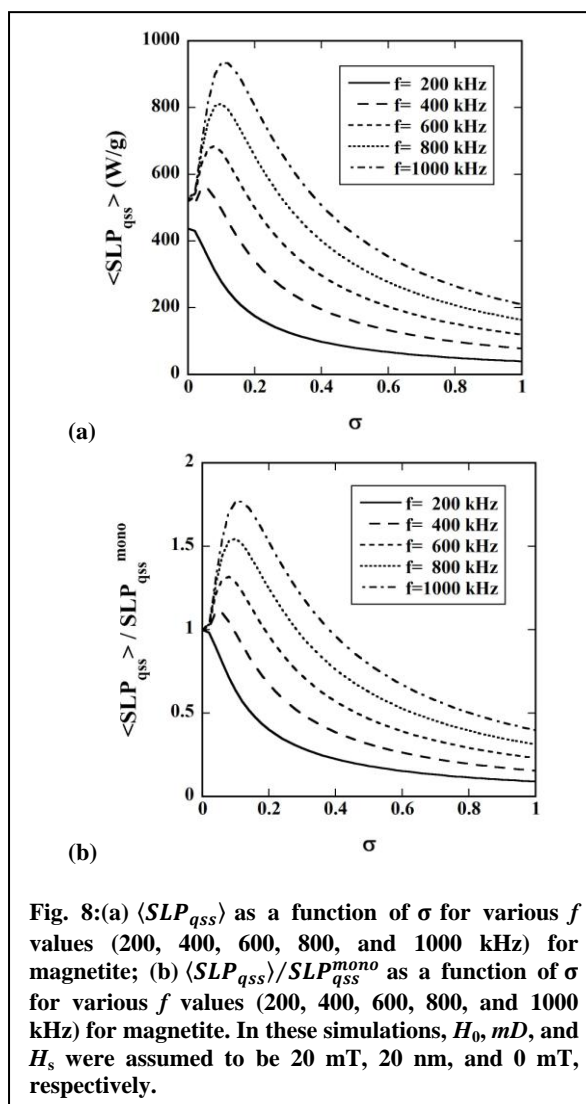


**Fig. 8:**(a)  $\langle SLP_{qss} \rangle$  as a function of  $\sigma$  for various  $f$  values (200, 400, 600, 800, and 1000 kHz) for magnetite; (b)  $\langle SLP_{qss} \rangle / SLP_{qss}^{mono}$  as a function of  $\sigma$  for various  $f$  values (200, 400, 600, 800, and 1000 kHz) for magnetite. In these simulations,  $H_0$ ,  $mD$ , and  $H_s$  were assumed to be 20 mT, 20 nm, and 0 mT, respectively.

parameter for evaluating the effect of size polydispersity on SLP.

As shown in Fig. 5 and Fig. 6,  $\langle SLP_{qss} \rangle / SLP_{qss}^{mono}$  did not change largely depending on  $H_0$ . Similarly, the dependency of  $\langle SLP_{qss} \rangle / SLP_{qss}^{mono}$  on  $H_s$  was not large (Fig. 9 and Fig. 10). As shown in Fig. 7 and Fig. 8, however,  $\langle SLP_{qss} \rangle / SLP_{qss}^{mono}$  changed largely depending on  $f$ . Furthermore, its dependency on  $f$  differed between maghemite and magnetite.  $H_0$  and  $f$  are usually determined by considering the safety, *i.e.*, the prevention of unwanted damage to the surrounding healthy tissue via eddy currents (typically their product  $H_0 \cdot f < 5 \times 10^9 \text{ Am}^{-1}\text{s}^{-1}$ ) [19]. The above results appear to suggest that the dependency of  $\langle SLP_{qss} \rangle / SLP_{qss}^{mono}$  on  $f$  can also be one of the important factors in selecting  $f$  for enhancing the therapeutic efficacy of magnetic hyperthermia without unwanted damage to the surrounding healthy tissue. In other words, it might be possible to enhance the SLP in magnetic hyperthermia by controlling the particle size polydispersity depending on  $f$ .

Khandhar *et al.* [20] developed a comprehensive protocol for synthesizing highly

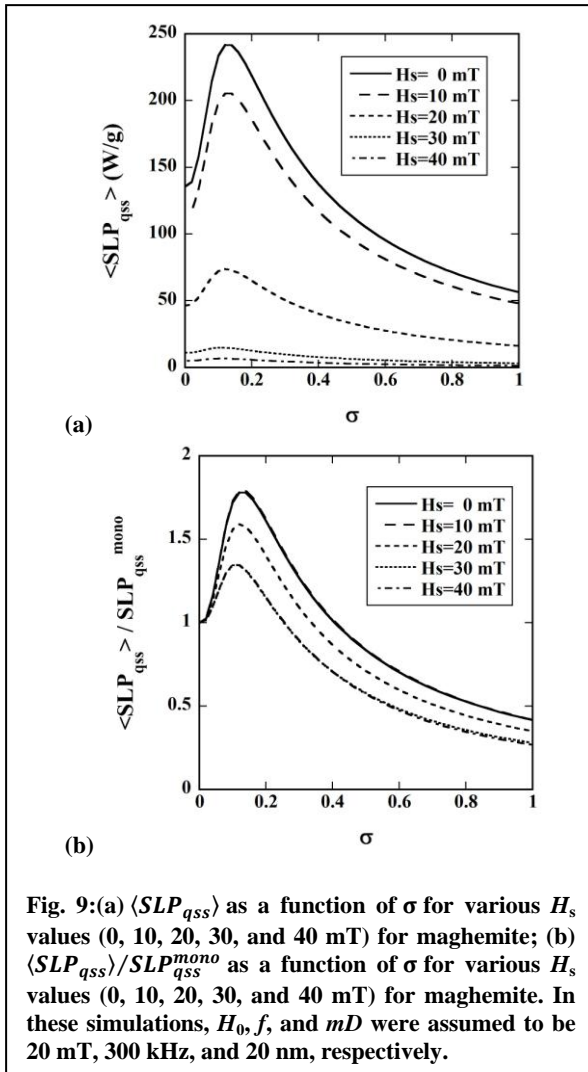


Fig. 9:(a)  $\langle SLP_{qss} \rangle$  as a function of  $\sigma$  for various  $H_s$  values (0, 10, 20, 30, and 40 mT) for maghemite; (b)  $\langle SLP_{qss} \rangle / SLP_{qss}^{mono}$  as a function of  $\sigma$  for various  $H_s$  values (0, 10, 20, 30, and 40 mT) for maghemite. In these simulations,  $H_0, f$ , and  $mD$  were assumed to be 20 mT, 300 kHz, and 20 nm, respectively.

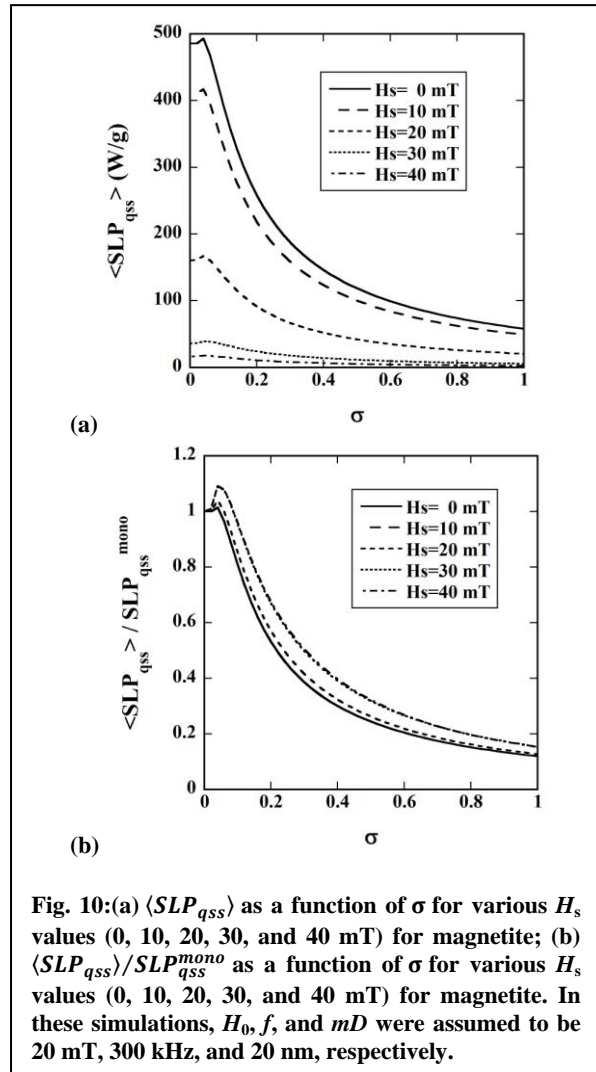


Fig. 10:(a)  $\langle SLP_{qss} \rangle$  as a function of  $\sigma$  for various  $H_s$  values (0, 10, 20, 30, and 40 mT) for magnetite; (b)  $\langle SLP_{qss} \rangle / SLP_{qss}^{mono}$  as a function of  $\sigma$  for various  $H_s$  values (0, 10, 20, 30, and 40 mT) for magnetite. In these simulations,  $H_0, f$ , and  $mD$  were assumed to be 20 mT, 300 kHz, and 20 nm, respectively.

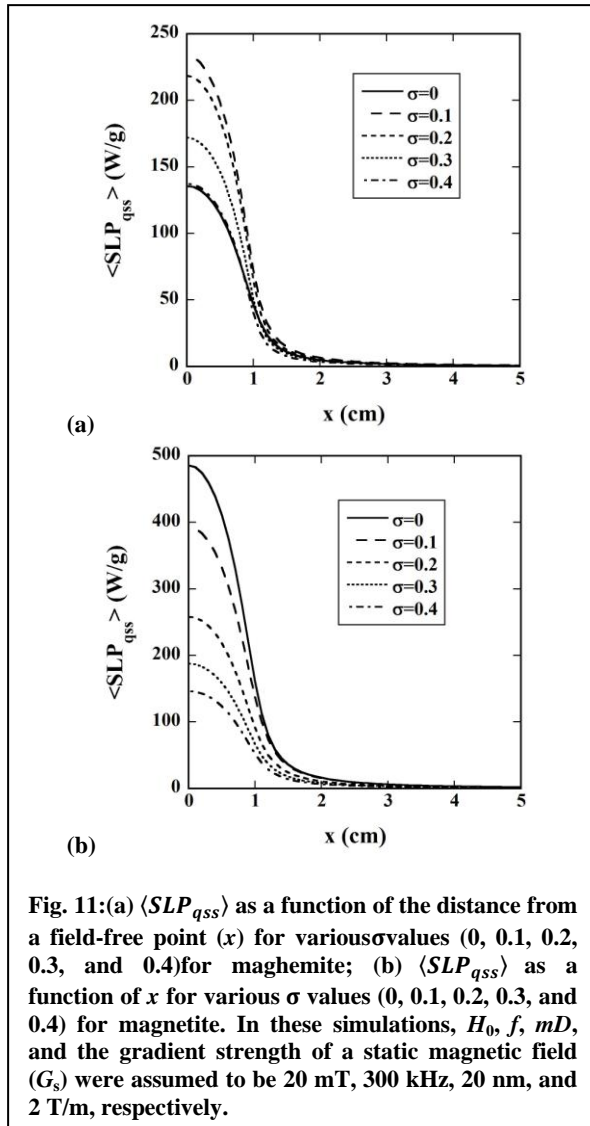
monodispersed MNPs and experimentally investigated the effect of particle size polydispersity on overall SLP. They reported that SLP values dropped by 30% with increased size polydispersity from  $\sigma = 0.175$  to  $\sigma = 0.266$  and emphasized the importance of monodispersity [20]. Gonzales-Weimuller *et al.* [21] reported that higher heating rates are achievable with iron oxides by decreasing polydispersity of the ferrofluid. However, it is worth noting that the opposite trend, *i.e.*, enhancement of the heating performance with higher polydispersity, has also been reported [13],[22]. Our results suggest that both cases can occur depending on the magnetic and physical properties of MNPs and/or the parameters of AMF.

As shown in Fig. 11, the plot of  $\langle SLP_{qss} \rangle$  against  $x$  changed largely depending on  $\sigma$  and its dependency on  $\sigma$  differed between maghemite and magnetite. These findings will be important in considering the control of the temperature rise and the area of local heating in magnetic hyperthermia by use of the SMF [9], [10].

In this study, we derived Eq. (13) by solving the magnetization relaxation equation of Shliomis [12] (Eq. (1)) with an assumption that there is no bulk flow and the magnetization of MNPs and magnetic field are

collinear. In this case, Eq. (1) is reduced to Eq. (2), which can be easily solved using convolution integral as shown in Eq. (9). Although Eq. (2) appears to be valid in considering the magnetic hyperthermia with small MNPs in the superparamagnetic state, it will be necessary to solve Eq. (1) without any assumptions or another magnetization equation derived microscopically from the Fokker-Planck equation [15] for more detailed analysis. Dhavalikar *et al.* [23] used the phenomenological magnetization equation derived by Martsenyuk *et al.* [24] instead of the Shliomis' equation [12] used in this study. The comparative studies between the present results with those obtained by the equation of Martsenyuk *et al.* [24] are currently in progress. Furthermore, we targeted the MNPs consisting of maghemite and magnetite with the magnetic and physical properties described in the "Simulation Studies" section. We will also perform further studies for the MNPs with other magnetic and physical properties and/or other MNPs.

In this study, we investigated the effect of particle size polydispersity on the heating performance of MNPs from a global point of view. For more detailed analysis, it might be necessary to investigate it at a local level using methods such as a Monte Carlo



technique [13], [14]. Studies using the Monte Carlo technique are currently planned.

## V. CONCLUSIONS

We investigated the effect of particle size polydispersity on the SLP in magnetic hyperthermia in comparison with the monodisperse case under various conditions of MNPs, AMF, and SMF. Our results demonstrated that the particle size polydispersity largely affects the SLP in magnetic hyperthermia and suggest that it is essential to take it into account for the accurate estimation of SLP and for accurately controlling the temperature rise and the area of local heating in magnetic hyperthermia using the SMF.

## ACKNOWLEDGMENT

This work was supported by a Grant-in-Aid for Scientific Research (Grant Number: 25282131 and 15K12508) from the Japan Society for the Promotion of Science (JSPS).

## REFERENCES

[1] A. Jordan, R. Scholz, K. Maier-Hauff, M. Johannsen, P. Wust, J. Nodobny, H. Schirra, H. Schmidt, S. Deger, S. Loening, W.

Lanksch, and R. Felix, "Presentation of a new magnetic field therapy system for the treatment of human solid tumors with magnetic fluid hyperthermia," *J. Magn. Magn. Mater.*, vol. 225, pp. 118-126, 2001.

[2] K. Murase, M. Aoki, N. Banura, K. Nishimoto, A. Mimura, T. Kuboyabu, and I. Yabata, "Usefulness of magnetic particle imaging for predicting the therapeutic effect of magnetic hyperthermia," *Open J. Med. Imaging*, vol. 5, pp. 85-99, 2015.

[3] T. Kuboyabu, I. Yabata, M. Aoki, N. Banura, K. Nishimoto, A. Mimura, and K. Murase, "Magnetic particle imaging for magnetic hyperthermia treatment: visualization and quantification of the intratumoral distribution and temporal change of magnetic nanoparticles *in vivo*," *Open J. Med. Imaging*, vol. 6, pp. 1-15, 2016.

[4] T. Neuberger, B. Schopf, H. Hofmann, M. Hofmann, and B. von Rechenberga, "Superparamagnetic nanoparticles for biomedical applications: possibilities and limitations of a new drug delivery system," *J. Magn. Magn. Mater.*, vol. 293, pp. 483-496, 2005.

[5] S. Maruyama, K. Shimada, K. Enmeiji, and K. Murase, "Development of magnetic nanocarriers based on thermosensitive liposomes and their visualization using magnetic particle imaging," *Int. J. Nanomed. Nanosurg.*, vol. 2, pp. 1-11, 2016.

[6] J. H. Lee, J. T. Jang, J. S. Choi, S. H. Moon, S. H. Noh, J. W. Kim, I. S. Kim, K. I. Park, and J. Cheon, "Exchange-coupled magnetic nanoparticles for efficient heat induction," *Nat. Nanotechnol.*, vol. 6, pp. 418-422, 2011.

[7] R. E. Rosensweig, "Heating magnetic fluid with alternating magnetic field," *J. Magn. Magn. Mater.*, vol. 252, pp. 370-374, 2002.

[8] K. Murase, "Methods for estimating specific loss power in magnetic hyperthermia revisited," *Open J. Appl. Sci.*, vol. 6, pp. 815-825, 2016.

[9] T. O. Tasci, I. Vargel, A. Arat, E. Guzel, P. Korkusuz, and E. Atalar, "Focused RF hyperthermia using magnetic fluids," *Med. Phys.*, vol. 36, pp. 1906-1912, 2009.

[10] K. Murase, H. Takata, Y. Takeuchi, and S. Saito, "Control of the temperature rise in magnetic hyperthermia with use of an external static magnetic field," *Phys. Med.*, vol. 29, pp. 624-630, 2013.

[11] K. Murase, "A simulation study on the specific loss power in magnetic hyperthermia in the presence of a static magnetic field," *Open J. Appl. Sci.*, vol. 6, pp. 839-851, 2016.

[12] M. I. Shliomis, "Effective viscosity of magnetic suspensions," *Sov. Phys. JETP*, vol. 34, pp. 1291-1294, 1972.

[13] C. Munoz-Menendez, I. Conde-Leboran, D. Baldomir, O. Chubykalo-Fesenko, and D. Serantes, "The role of size polydispersity in magnetic fluid hyperthermia: average vs. local infra/over-heating effects," *Phys. Chem. Chem. Phys.*, vol. 17, pp. 27812-27820, 2015.

[14] C. Munoz-Menendez, I. Conde-Leboran, D. Serantes, R. Chantrell, O. Chubykalo-Fesenko, and D. Baldomir, "Distinguishing between heating power and hyperthermic cell-treatment efficacy in magnetic fluid hyperthermia," *Soft Matter*, vol. 12, pp. 8815-8818, 2016.

[15] D. Soto-Aquino and C. Rinaldi, "Magnetoviscosity in dilute ferrofluids from rotational brownian dynamics simulations," *Phys. Rev. E*, vol. 82, Article ID: 046310, 2010.

[16] W. H. Press, S. A. Teukolsky, W. T. Vetterling, and B. P. Flannery, *Numerical Recipes in C*, Oxford, United Kingdom: Cambridge University Press, 1992.

[17] K. Murase, J. Oonoki, H. Takata, R. Song, A. Angraini, P. Ausanai, and T. Matsushita, "Simulation and experimental studies on magnetic hyperthermia with use of superparamagnetic iron oxide nanoparticles," *Radiol. Phys. Technol.*, vol. 4, pp. 194-202, 2011.

[18] S. Maenosono and S. Saita, "Theoretical assessment of FePt nanoparticles as heating elements for magnetic hyperthermia," *IEEE Trans. Magn.*, vol. 42, pp. 1638-1642, 2006.

[19] R. Hergt and S. Dutz, "Magnetic particle hyperthermia — biophysical limitations of a visionary tumour therapy," *J. Magn. Magn. Mater.*, vol. 311, pp. 187-192, 2007.

- [20] A. P. Khandhar, R. M. Ferguson, and K. M. Krishnana, "Monodispersed magnetite nanoparticles optimized for magnetic fluid hyperthermia: implications in biological systems," *J. Appl. Phys.*, vol. 109, Article ID: 07B310, 2011.
- [21] M. Gonzales-Weimuller, M. Zeisberger, and K. M. Krishnan, "Size-dependant heating rates of iron oxide nanoparticles for magnetic fluid hyperthermia," *J. Magn. Magn. Mater.*, vol. 321, pp. 1947-1950, 2009.
- [22] M. Jeun, S. Bae, A. Tomitaka, Y. Takemura, K. H. Park, S. H. Paek, and K-W. Chung, "Effects of particle dipole interaction on the AC magnetically induced heating characteristics of ferrite nanoparticles for hyperthermia," *Appl. Phys. Lett.*, vol. 95, Article ID: 082501, 2009.
- [23] R. Dhavalikar and C. Rinaldi, "Theoretical predictions for spatially-focused heating of magnetic nanoparticles guided by magnetic particle imaging field gradients," *J. Magn. Magn. Mater.*, vol. 419, pp. 267-273, 2016.
- [24] M. A. Martsenyuk, Y. L. Raikher, and M. I. Shliomis, "On the kinetics of magnetization of ferromagnetic particle suspension," *Sov. Phys. JETP*, vol. 38, pp. 413-416, 1974.